Vehicle Yaw Inertia and Mass Independent Adaptive Control for Stability and Trajectory Tracking Enhancements

Junmin Wang* and Ming Feng Hsieh

Department of Mechanical Engineering
The Ohio State University
Columbus, Ohio 43210

Abstract — This paper describes a vehicle stability control (VSC) system using a yaw inertia and mass independent adaptive control law. As a primary vehicle active control system, VSC can significantly improve vehicle driving safety for passenger cars and enhance trajectory tracking accuracy for other applications such as autonomous, surveillance, and wheeled mobile robot vehicles. For the designs of vehicle dynamic control systems, vehicle yaw inertia and mass are two of the most important parameters. However, in practical applications, vehicle yaw inertia and mass often change with vehicle payload and load distribution. In this paper, an adaptive control law is proposed to treat the vehicle yaw inertia and mass as unknown parameters and automatically address their variations. For the proposed adaptive control law, asymptotical stability of the yaw rate tracking error was proved by a Lyapunov-like analysis for certain vehicle architecture under some reasonable assumptions. The performance of the yaw inertia and mass independent adaptive vehicle stability control system was evaluated under several driving conditions (i.e. double lane-changing on a slippery surface and brake on a split-µ surface tests) through simulation studies using a high-fidelity full-vehicle model provided by CarSim®.

I. INTRODUCTION

VEHICLE stability control has been an active research area in both academia and industry for several decades and is still evolving rapidly thanks to the ever-growing sensing, actuation, and control technologies [1-9]. While majority of the VSC research and development efforts have been focused on passenger car applications for safety enhancement reasons, the VSC technology has also been introduced into categories such as surveillance, unmanned patrol, autonomous, wheeled mobile robot, and other special vehicles to enhance their performance and trajectory tracking capabilities [10-13]. For some VSC passenger car applications, variations of vehicle parameters such as sprung mass may be insignificant due to the relatively small payload changes compared with the vehicle mass. However, for lightweight vehicle applications such as autonomous, wheeled mobile robot, and surveillance

vehicles, the vehicle payload variations could be quite substantial and sometime even well exceed the masses of the vehicle themselves. For wheeled mobile robots and surveillance vehicles such as autonomous mine detectors/cleaners, vehicle weight/load distributions oftentimes change during operations. Consequently, important vehicle system parameters (i.e. vehicle mass and yaw inertia) could vary considerably during routine operations and these parametric variations may affect the vehicle control performance such as stability and trajectory tracking especially at high-speed operation. Yaw rate is commonly designed as the main control objective for many VSC control systems, in which the vehicle yaw inertia and mass are two of the important parameters for control algorithms [1, 5, 9, 11, 17]. For example, in some VSC algorithms, controller gains may depend on the values of the vehicle yaw inertia and mass. In cases where the vehicle yaw inertias and mass change noticeably, it is desirable for the VSC control algorithms to automatically and appropriately accommodate those variations in order to ensure the satisfactory control performance at different operating conditions. In this paper, we attempt to tackle the problem of the vehicle yaw inertia/mass variations by using a yaw inertia and mass independent adaptive control law.

The rest of the paper is organized as follows. In Section II, vehicle planar motion dynamic model is briefly presented. The vehicle yaw inertia and mass adaptive control law is designed in Section III. Simulation results are presented in Section IV followed by conclusive remarks and future work summarized in Section V.

II. SYSTEM MODELING

For ground vehicles, the planar dynamic motion (longitudinal, lateral, and yaw) are commonly considered as the most critical control objectives. The vehicle can be modeled as a rigid body with three degrees-of-freedom. Figure 1 shows the vehicle diagram under planar dynamic motion.
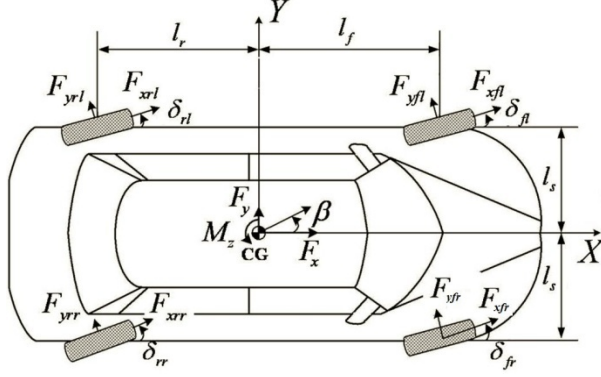
*Tel: 614-247-7275; Email: wang.1381@osu.edu.

Fig. 1. The ground vehicle planar dynamic motions

The simplified vehicle planar dynamic equations of motion can be simplified as

$$m_v(\dot{V}_x - rV_y) = F_x$$
$$m_v(\dot{V}_y + rV_x) = F_y \quad ,\qquad (1)$$
$$\dot{r} = \frac{1}{I_{zz}}M_z$$

where m_v is the vehicle mass (including both sprung and unsprung mass), V_x is vehicle velocity along the X axis, V_y is vehicle velocity along the Y axis, and I_{zz} is vehicle moment of inertia about the Z axis, which is perpendicular to the x-y plane. The coordinates X, Y, Z are body-fixed at the vehicle center of gravity (C.G.). The generalized external forces acting along the vehicle X and Y axes are F_x and F_y, respectively. The generalized external moment about the Z axis is M_z. Ultimately, each of the four wheels can independently drive, brake, and steer. Thus, these generalized forces/moment are expressed as [6],

$$F_x = F_{xfl}\cos\delta_{fl} - F_{yfl}\sin\delta_{fl} + F_{xfr}\cos\delta_{fr} - F_{yfr}\sin\delta_{fr}$$
$$+ F_{xrl}\cos\delta_{rl} - F_{yrl}\sin\delta_{rl} + F_{xrr}\cos\delta_{rr} - F_{yrr}\sin\delta_{rr} \quad ,(2a)$$

$$F_y = F_{xfl}\sin\delta_{fl} + F_{yfl}\cos\delta_{fl} + F_{xfr}\sin\delta_{fr} + F_{yfr}\cos\delta_{fr}$$
$$+ F_{xrl}\sin\delta_{rl} + F_{yrl}\cos\delta_{rl} + F_{xrr}\sin\delta_{rr} + F_{yrr}\cos\delta_{rr} \quad ,(2b)$$

$$M_z = l_s(-F_{xfl}\cos\delta_{fl} + F_{yfl}\sin\delta_{fl} - F_{xrl}\cos\delta_{rl} + F_{yrl}\sin\delta_{rl})$$
$$+ l_s(F_{xfr}\cos\delta_{fr} - F_{yfr}\sin\delta_{fr} + F_{xrr}\cos\delta_{rr} - F_{yrr}\sin\delta_{rr}) \quad .(2c)$$
$$+ l_f(F_{xfl}\sin\delta_{fl} + F_{yfl}\cos\delta_{fl} + F_{xfr}\sin\delta_{fr} + F_{yfr}\cos\delta_{fr})$$
$$+ l_r(-F_{xrl}\sin\delta_{rl} - F_{yrl}\cos\delta_{rl} - F_{xrr}\sin\delta_{rr} - F_{yrr}\cos\delta_{rr})$$

In these relations, δ_{**} is the steering angle of a given wheel, with the first subscript representing front/rear and the second subscript indicating right/left. In this paper, we only consider controlling the vehicle yaw rate and assume that the vehicle speed will be controlled by a separate speed controller or by a driver.

Note that during normal operations (when tires work in the linear ranges), tire longitudinal and lateral forces can be approximately described by the following linear model [14, 15],

$$F_{xi} = F_{zi}K_x(\mu_i)s_i \,, \qquad (3)$$
$$F_{yi} = F_{zi}K_y(\mu_i)\alpha_i \,, \qquad (4)$$

where $K_x(\mu_i)$ and $K_y(\mu_i)$ are constants (that define the slops of the tire slip and slip angle vs. longitudinal and lateral forces, respectively.) as a function of maximum available tire-road friction coefficient, μ_i, which can be estimated using some on-line estimators such as the ones described in [14, 15]. Note that the above simple linear tire model is valid only when tire is not experiencing both longitudinal and lateral forces simultaneously.

For vehicles in which 4-wheel driving/steering are not available, then we can have $\delta_{fl} = \delta_{fr} = \delta_s$ and $\delta_{rl} = \delta_{rr} = 0$. For the vehicles that are rear-wheel-drive only, we can ignore the longitudinal forces of the front tires and assume the longitudinal forces of the rear tires are approximately the same. Thus we can reformulate the yaw moment (2c) as,

$$M_z = l_s\sin\delta_s(F_{yfl} - F_{yfr}) + l_f\cos\delta_s(F_{yfl} + F_{yfr}) - l_r(F_{yrl} + F_{yrr}). \quad (5)$$

In normal steering angle range, δ_s is small. So we can have $\cos\delta_s \approx 1$ and ignore the first term in (5). Thus we arrived at,

$$M_z \approx -l_r(F_{yrl} + F_{yrr}) + l_f\left[F_{zfl}K_y(\mu)\alpha_{fl} + F_{zfr}K_y(\mu)\alpha_{fr}\right]$$
$$= -l_r(F_{zrl}K_y(\mu)\alpha_{rl} + F_{zrr}K_y(\mu)\alpha_{rr})$$
$$+ l_fF_{zfl}K_y(\mu)\mathrm{atan}\left(\frac{V_y + rl_f}{V_x - rl_s}\right)$$
$$+ l_fF_{zfr}K_y(\mu)\mathrm{atan}\left(\frac{V_y + rl_f}{V_x + rl_s}\right)$$
$$- \frac{l_f}{R_s}\left[F_{zfl}K_y(\mu) + F_{zfr}K_y(\mu)\right]\delta_{sw}$$
$$= m_v\left\{-l_r\left(\frac{gl_f}{2(l_f + l_r)}K_y(\mu)\alpha_{rl} + \frac{gl_f}{2(l_f + l_r)}K_y(\mu)\alpha_{rr}\right)\right.$$
$$+ \frac{gl_rl_f}{2(l_f + l_r)}K_y(\mu)\mathrm{atan}\left(\frac{V_y + rl_f}{V_x - rl_s}\right)$$
$$+ \frac{gl_rl_f}{2(l_f + l_r)}K_y(\mu)\mathrm{atan}\left(\frac{V_y + rl_f}{V_x + rl_s}\right) \qquad ,(6)$$
$$\left. - \frac{l_f}{R_s}\left[\frac{gl_r}{2(l_f + l_r)}K_y(\mu) + \frac{gl_r}{2(l_f + l_r)}K_y(\mu)\right]\delta_{sw}\right\}$$

where R_s is the steering mechanism gear ratio. Here we ignore the tire normal load dynamic transfer, which is considerable only during severe turns. Consequently, we can have

$$M_z \approx m_vh(\cdot), \qquad (7)$$

where $h(\cdot)$ is the part within the braces in (6). By substituting (7) into (1), one can get,

$$\dot{r} = \frac{1}{I_{zz}/m_v} h(\cdot) = \frac{1}{I} h(\cdot) . \tag{8}$$

Define $I = I_{zz}/m_v$ as a lumped parameter of the vehicle yaw inertia and mass. Both vehicle yaw inertia and mass commonly vary with payload and load/weight distributions and so does the parameter I.

III. DESIGN OF THE ADAPTIVE CONTROL LAW

For the vehicle yaw motion dynamical model as described in the foregoing section, we can develop a vehicle yaw inertia and mass independent adaptive control law with the front wheel steering being the control actuation.

Define the yaw rate tracking error as the difference between the measured actual vehicle yaw rate and the desired one as:

$$e = r - r_d, \tag{9}$$

where r_d is the desired yaw rate, which needs to be sufficiently smooth with its time-derivative bounded and can be generated from a driver model by using the steering hand-wheel and vehicle speed as the inputs [4, 7] or from the desired vehicle travel trajectory and measured vehicle position as described in [10, 11]. The error dynamics is then given by,

$$\begin{aligned}
\dot{e} = \dot{r} - \dot{r}_d &= \frac{1}{I} h(\cdot) - \dot{r}_d \\
&= ae - ae + \frac{1}{I} h(\cdot) - \dot{r}_d \\
&= -ae + \frac{1}{I} \left[h(\cdot) - I(\dot{r}_d - ae) \right]
\end{aligned} \tag{10}$$

Let $\theta^* = I$ represent the true value of the vehicle yaw inertia divided by vehicle mass, and $\hat{\theta}$ be the estimation of θ^*. We define the estimation error as $\tilde{\theta} = \hat{\theta} - \theta^*$. Then we can rewrite the yaw rate tracking error dynamics as,

$$\dot{e} = -ae + \frac{1}{I} \left[h(\cdot) - \theta^*(\dot{r}_d - ae) \right]. \tag{11}$$

The following adaptive control law can then ensure the asymptotical stability of the yaw rate tracking error.

$$h(\cdot) = \hat{\theta}(\dot{r}_d - ae), \tag{12}$$

with the following estimation update law

$$\dot{\hat{\theta}} = -k(\dot{r}_d - ae)e, \tag{13}$$

where, $a \in \Re^+$ and $k \in \Re^+$. The initial value for the estimation, $\hat{\theta}_0$, can be any value.

Proof: The proof of the asymptotical stability of the tracking error was conducted by a Lyapunov-like analysis [18]. Substituting (12) into (11), the error dynamics became

$$\dot{e} = -ae + \frac{1}{I}\tilde{\theta}(\dot{r}_d - ae). \tag{14}$$

Consider the following Lyapunov function candidate,

$$V = \frac{1}{2}e^2 + \frac{1}{2Ik}\tilde{\theta}^2 . \tag{15}$$

It is obviously positive semi-definite. Its derivative is given by

$$\begin{aligned}
\dot{V} &= e\dot{e} + \frac{1}{Ik}\tilde{\theta}\dot{\tilde{\theta}} \\
&= -ae^2 + \frac{1}{I}e\tilde{\theta}(\dot{r}_d - ae) + \frac{1}{Ik}\tilde{\theta}\dot{\hat{\theta}} \\
&= -ae^2 + \frac{1}{I}e\tilde{\theta}(\dot{r}_d - ae) + \frac{1}{Ik}\tilde{\theta}\left[-k(\dot{r}_d - ae)e \right] \\
&= -ae^2 \\
&\le 0
\end{aligned} \tag{16}$$

Since we have $V \ge 0$ and $\dot{V} \le 0$, then we know that $V \in L_\infty \Rightarrow e, \tilde{\theta} \in L_\infty \Rightarrow \hat{\theta} \in L_\infty$. Also, we can have that $\underset{t\to\infty}{Lim} V \triangleq V_\infty$ exists and is finite. So, if we integrate both sides of (16), we can then obtain the following property,

$$\underset{t\to\infty}{Lim} \int_0^t \dot{V} d\tau = \underset{t\to\infty}{Lim} \int_0^t -ae^2 d\tau = V_\infty - V(0) . \tag{17}$$

Thus, $\underset{t\to\infty}{Lim} \int_0^t -ae^2 d\tau$ exists and is finite. It therefore gives that $e \in L_\infty \cap L_2$. On the other hand, from (14) it is obvious that $\dot{e} \in L_\infty$. We can then conclude that $\underset{t\to\infty}{Lim} e = 0$ by Barbalat's Lemma. Thus, by using the adaptive control law described in (12), the yaw rate tracking error will be asymptotically stable or goes to zero with time. ∎

One can see that neither the vehicle yaw inertia nor vehicle mass is used in the adaptive control law (12) or the estimation updating law (13). So, the control law is independent of both the vehicle yaw inertia and mass values.

Once $h(\cdot)$ is specified by the adaptive control law (12) and (13), the steering hand-wheel angle can be obtained from (6) and (7) as,

$$\delta_{sw} = \left\{ gl_r l_f K_y(\mu) \left[a\tan\left(\frac{V_y + rl_f}{V_x - rl_s}\right) + a\tan\left(\frac{V_y + rl_f}{V_x + rl_s}\right) \right] - \alpha_{rl} - \alpha_{rr} \right. \\ \left. - 2(l_f + l_r)\hat{\theta}(\dot{r}_d - ae) \right\} / \left[2\frac{K_y(\mu)}{R_s} gl_f l_r \right] . \tag{18}$$

In the vehicle front wheel steering angle control law given by (18), all the parameters/coefficients are measureable with advanced vehicle sensing systems such as GPS/IMU systems etc. [9, 15]. Even though these advanced sensing systems are still not widely available on commercial vehicles yet, they could be equipped on other specific applications such as autonomous and military surveillance vehicles.

IV. SIMULATION STUDIES

The designed adaptive VSC control system was evaluated in Matlab-CarSim® co-simulation. CarSim is a high-fidelity full-vehicle multibody dynamics (including complex and accurate tire models) simulation package that can produce response characteristics which have shown favorable comparison with experimental data taken from real vehicles [16]. The main vehicle parameter values used for the CarSim full-vehicle simulation models are listed in Table 1. Two different vehicles, high-I and low-I with different I (I_{zz}/m_v) values (2.73 and 1.2), are considered in the simulations. Note that the yaw inertia was used for configuring the vehicle simulation model only but not used in the control law. Simulation using the full-vehicle model also provides evaluation of the robustness of the adaptive control law to unmodeled dynamics. The initial value of I was set as 2.0 in the adaptive control law. Vehicle mass and yaw inertia typically change in the same direction. Vehicle yaw inertia usually increases/decreases with increasing/decreasing vehicle mass. However, for some special cases such as wheeled mobile robots, vehicle load/mass may be redistributed during operation and the redistributions may cause yaw inertia to increase or decrease regardless of the vehicle mass changes. For this consideration, the high-I and low-I vehicles in the simulation were made by changing the vehicle mass and yaw inertia in opposite directions as shown in Table 1.

Table 1. CarSim vehicle simulation model parameters

	High-I Veh.	Low-I Veh.
I (I_{zz}/m_v), (m^2)	2.73	1.20
Sprung mass, m_v, (kg)	1530	1830
Yaw inertia, I_{zz}, (kg-m^2)	4192	2192
Wheelbase (m)	2.776	2.776
Track (m)	1.55	1.55
C.G. Height (m)	0.54	0.54

Two different scenarios were used to show the effectiveness of the proposed vehicle yaw inertia and mass independent adaptive control law. One is a high-speed double lane changing (DLC) on a slippery surface and the other is a brake through a split-μ surface.

A. High-Speed Double Lane-Changing on a Slippery Surface

In this simulation, the vehicle initial speed was set as 120 km/h. Tire-road friction coefficient was 0.6. A double lane-changing command was issued at 1 second during the simulation. Identical adaptive VSC control law with same parameters were used for both high-I vehicle (red) and low-I vehicle (silver). Figure 2 shows the behaviors of the vehicles during the DLC maneuver. One can see that the control law helped the vehicles maintain closely tracking of the desired trajectory even during this severe maneuver. The two vehicles exhibited almost identical behaviors even though their yaw inertias and masses are quite different.
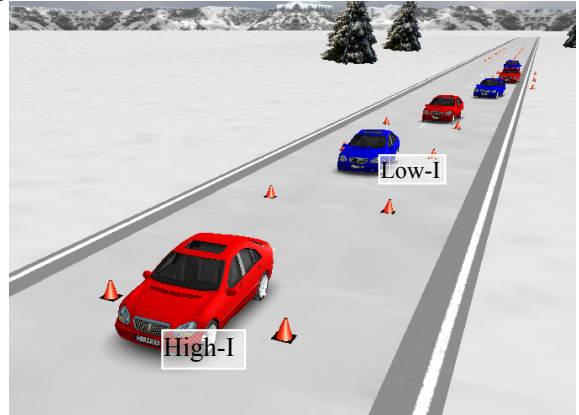

Fig. 2. Comparisons of vehicle behaviors during a DLC maneuver (red car: high-I vehicle; silver car: low-I vehicle).

Vehicle global trajectories and the steering hand-wheel angles were plotted in Figure 3 and Figure 4, respectively. Figure 5 illustrates the vehicle yaw rate responses compared with the desired one during the DLC maneuver. The yaw inertia and mass adaptive control law can make the vehicles track the desired yaw rate as shown in Figure 5, and consequently the vehicles were able to follow the desired trajectory closely as shown in Figure 3. It is noticeable that the adaptive control law automatically applied greater control effort for the vehicle with high I value during the maneuver.
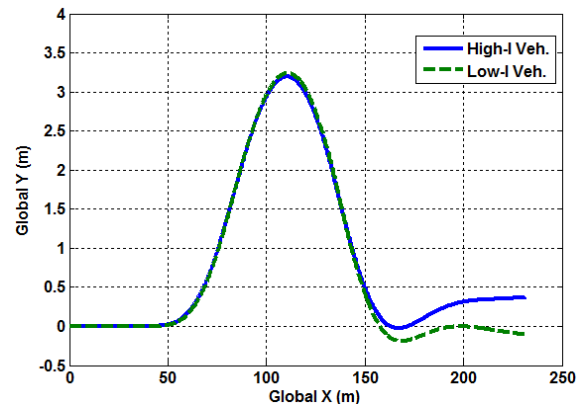

Fig. 3. Comparisons of the vehicle global trajectories during the DLC maneuver.
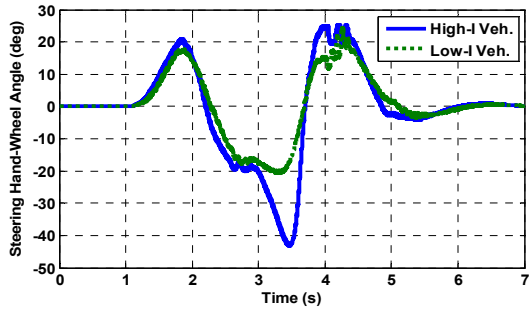
Fig. 4. Comparisons of the vehicle steering angles during the DLC maneuver.
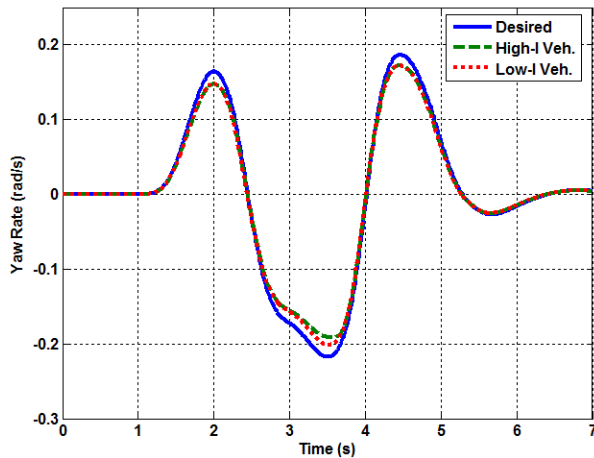

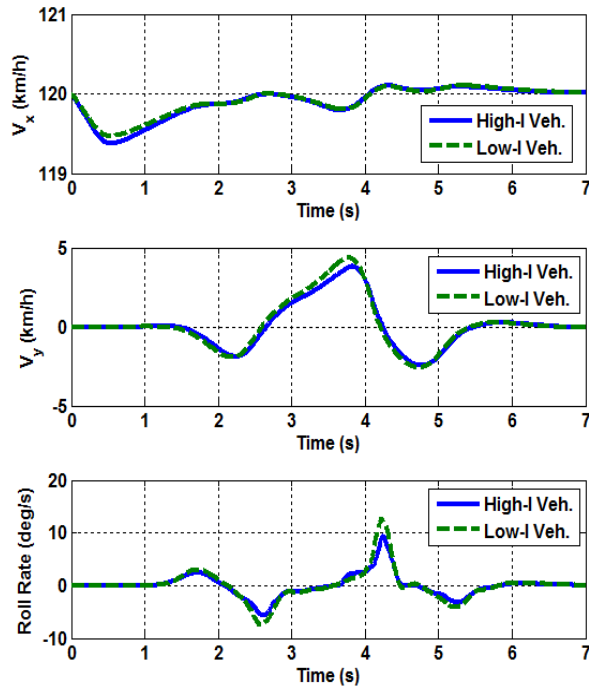Fig. 5. Comparisons of the vehicle yaw rate responses during the DLC maneuver.

Fig. 6. Comparisons of the vehicle longitudinal speeds, lateral speeds, and roll rates during the DLC maneuver.

As shown in Figure 6, very similar longitudinal speed, lateral speed, and roll rate responses were achieved for both vehicles during the maneuver.

B. Braking through a Split-μ Surface

The second simulation case is braking through a split-μ surface whose left side friction coefficient was 0.2 and right side friction coefficient was 0.5. Three vehicles were compared in this case, the high-I and low-I vehicles with the adaptive steering control and a high-I vehicle without steering action. Anti-lock brake systems were active for all three vehicles during the simulation. The initial speed of the vehicles was 80 km/h and a hard brake command was issued at the beginning of the simulation. Figure 7 shows the vehicle behaviors during this maneuver.
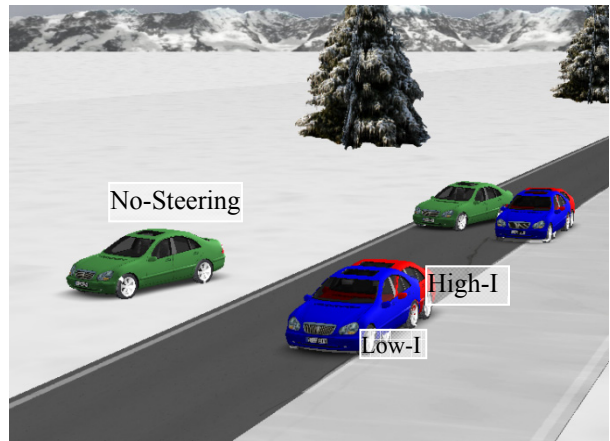

Fig.7. Vehicle behaviors during the braking on a split-μ surface (red car: high-I vehicle; blue car: low-I vehicle; green car: vehicle without steering action).

Vehicle longitudinal speeds and global trajectories are depicted in Figure 8 and Figure 9, respectively. From these figures, one can observe that the adaptive VSC assisted the vehicle in maintaining on the desired track during this adverse maneuver.
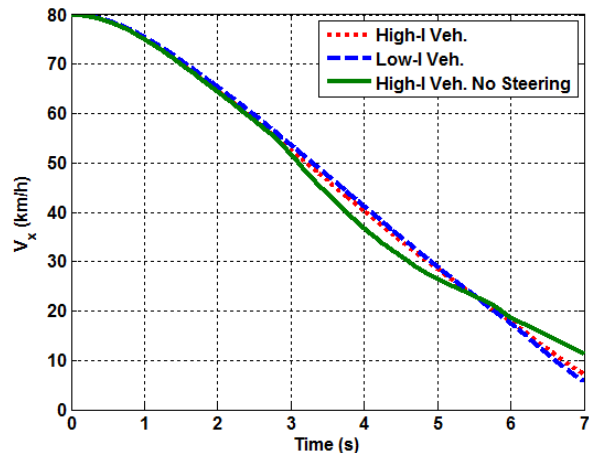

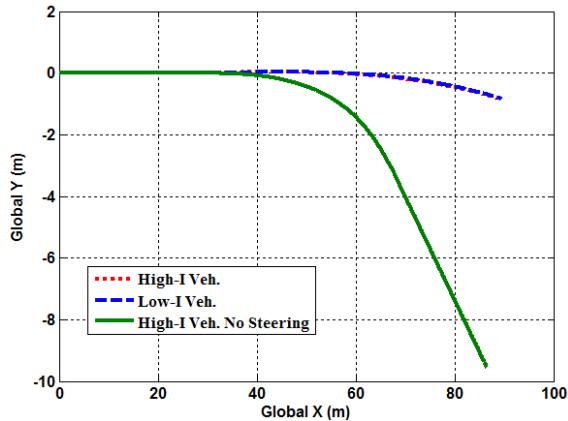Fig. 8. Vehicle longitudinal speeds during the braking on a split-μ surface maneuver.

693

Fig. 9. Vehicle global trajectories during the braking on a split-μ surface maneuver.

V. Conclusions and Future Work

A vehicle yaw inertia and mass independent adaptive VSC control system is proposed to deal with the yaw inertia and vehicle mass variations that are commonly encountered for various ground vehicle applications. The asymptotical stability of the proposed adaptive control law was proven based on a Lyapunov-like analysis for certain vehicle architecture. The effectiveness of the adaptive control law was evaluated in simulations using a high-fidelity full-vehicle model provided by CarSim®. By using the yaw inertia and mass independent VSC control law, performance deteriorations caused by the vehicle yaw inertia and/or mass variations can be automatically attenuated.

There are several related research topics that we are working on. The developed adaptive control law can only be applied to vehicles with front-steer-rear-drive architecture. It would be desirable to expand the application to vehicles with different architectures. In equation (7), we ignored the tire normal load dynamic transfer effect, which deserves further analysis and investigation. The tire-road friction coefficient was assumed as a constant in this paper. It would be valuable to further develop the control system which is capable of handling the tire-road friction coefficient variations as well. As vehicle load/mass redistribute, vehicle geometric parameters, such as C.G. location, might change too. Adaptation with regards to vehicle geometric parameters would be valuable as well.

References

[1] Y. Furukawa, N. Yuhara, S. Sano, H. Takeda, and Y. Matsushita, "A Review of Four-Wheel Steering Studies from the Viewpoint of Vehicle Dynamics and Control," *Vehicle System Dynamics*, Vol. 18, No. 1, pp. 151 – 186, 1989.

[2] K. Shimada and Y. Shibahata, "Comparison of three active chassis control methods for stabilizing yaw moments," *SAE Paper 940870*, 1994.

[3] M. Abe, "Vehicle dynamics and control for improving handling and active safety: from four-wheel steering to direct yaw moment control," *Proceedings of the Institute of Mechanical Engineers-Journal of Automobile Engineering*, Vol. 213, pp. 87-101, 1999.

[4] T. Shim and D. Margolis, "Using u Feedforward for Vehicle Stability Enhancement," *Vehicle System Dynamics*, Vol. 35, No. 2, pp. 103 – 119, 2001.

[5] J. Wang and R. Longoria, "Coordinated vehicle dynamics control with control distribution," *Proceedings of the American Control Conference*, pp. 5348-5353, 2006.

[6] D. Piyabongkarn, R. Rajamani, J. A. Grogg, and J. Y. Lew, "Development and Experimental Evaluation of a Slip Angle Estimator for Vehicle Stability Control," *Proceedings of the American Control Conference*, pp. 5366 – 5371, 2006.

[7] J. Wang, J. Solis, and R. Longoria, "On the control allocation for coordinated ground vehicle dynamics control systems," *Proceedings of the American Control Conference*, pp. 5724-5729, 2007.

[8] J. Wang and R. Longoria, "Combined tire slip and slip angle tracking control for advanced vehicle dynamics control systems," *Proceedings of the 45th IEEE Conference on Decision and Control*, pp. 1733-1738, 2006.

[9] J. Wang and R. Longoria, "Coordinated and Reconfigurable Vehicle Dynamics Control," *IEEE Transactions on Control Systems Technology* (to appear).

[10] J. Wang, J. Steiber, and B. Surampudi, "Autonomous ground vehicle control system for high-speed and safe operation," *Proceedings of the American Control Conference – Invited Sessions*, pp. 218 – 223, 2008.

[11] J. Wang, J. Steiber, and B. Surampudi, "Autonomous ground vehicle control system for high-speed and safe operation," *International Journal of Vehicle Autonomous Systems* (accepted).

[12] M. Kodaira, T. Ohtomo, A. Tanaka, M. Iwatsuki, and T. Ohuchi, "Obstacle Avoidance Travel Control of Robot Vehicle Using Neural Network," *Systems and Computers in Japan*, Vol. 27, No. 12, pp. 102 – 112, 2007.

[13] J. K. Ong, D. Kerr, and K. Bouazza-Marouf, "Design of a Semi-Autonomous Modular Robotic Vehicle for Gas Pipeline Inspection," *Proceedings of the Institution of Mechanical Engineers, Part I: Journal of Systems and Control Engineering*, Vol. 217, No. 2, pp. 109 – 122, 2003.

[14] J.-O. Hahn, R. Rajamani, L. Alexander, "GPS-Based Real-Time Identification of Tire-Road Friction Coefficient," *IEEE Transactions on Control Systems Technology*, Vol. 10, No. 3, pp. 331 – 343, 2002.

[15] J. Wang, L. Alexander, and R. Rajamani, "Friction Estimation on Highway Vehicles Using Longitudinal Measurements," *ASME Journal of Dynamic Systems, Measurement, and Control*, Vol. 126, Issue 2, pp. 265 – 275, 2004.

[16] Mechanical Simulation Corporation, *CarSim User Manual*, version 5.11, 2003.

[17] J. Lew, D. Piyabongkan, and J. Grogg, "Minimizing Dynamic Rollover Propensity With Electronic Limited Slip Differentials," *SAE Transactions-Journal of Passenger Cars: Mechanical Systems*, Vol. 115-6, pp. 1183 – 1190, 2007.

[18] S. Sastry and M. Bodson, "Adaptive Control: Stability, convergence, and Robustness," Prentice Hall, 1989.